Gyrokinetic investigation of microturbulence in the edge of ELM suppressed H-modes in ASDEX Upgrade

F. Rath[1], A. G. Peeters[1], W. Suttrop[2], B. Stefanoska[2], M. Willensdorfer[2], and ASDEX Upgrade Team[3]

1. *Physics Department, University of Bayreuth, 95440 Bayreuth, Germany*
2. *Max-Planck-Institut für Plasmaphysik, D-85740 Garching, Germany*
3. *T. Pütterich et al, 2026 Nucl. Fusion 66 116002*

Introduction: Edge localized mode (ELM) suppression through the application of magnetic perturbations (MPs) is a common technique to mitigate intolerable heat loads on the plasma facing components. Thereby, MPs cause a so-called density pump-out that reduces the pedestal top density below an empirical threshold [1] and leading to ELM suppression. Several experimental [2] (AUG) [3] (DIII-D) [4] (KSTAR) but also theoretical [5] works report turbulence signatures during ELM suppression and discuss the potential role of turbulent transport for the density pump-out. In this work the ELM suppressed AUG shot #34548 [2], which exhibits signatures of turbulent broadband density fluctuations on ion Larmor radius scale during the ELM suppressed phase, is investigated within a gyrokinetic study using GKW [6] and the potential role of slab ITG driven turbulence for the density pump-out is discussed.

Model: The local δf version of GKW [6] is applied with local plasma parameters taken from the reference surface $\Psi_{N,\mathrm{ref}} = 0.9844$ in the steep gradient zone (Fig. 1), where the broadband fluctuations are observed [2]. A radial position space representation together with a small radial box size of $L_\mathcal{X} = 6.774\ \rho_{\mathrm{th,ref}}$ ($\rho_{\mathrm{th,ref}}$ is the local thermal reference Larmor radius of the ions) and radial Dirichlet boundary conditions are applied to model the narrow steep gradient zone similar to Ref. [7]. The shaped geometry is modeled by a Miller-Extended-Harmonics (MXH) parameterization [8] and nonlinear turbulence simulations apply a simple Krook heat and particle source. A single ion species (deuterium) and electrons are included. All simulations are electromagnetic including fluctuations of the parallel magnetic vector potential $A_{1\parallel}$, while parallel magnetic field fluctuations $B_{1\parallel}$ are modeled through a modification of the curvature drift as described in [9]. Collisions are modeled through a linearized Fokker-Planck collision operator.

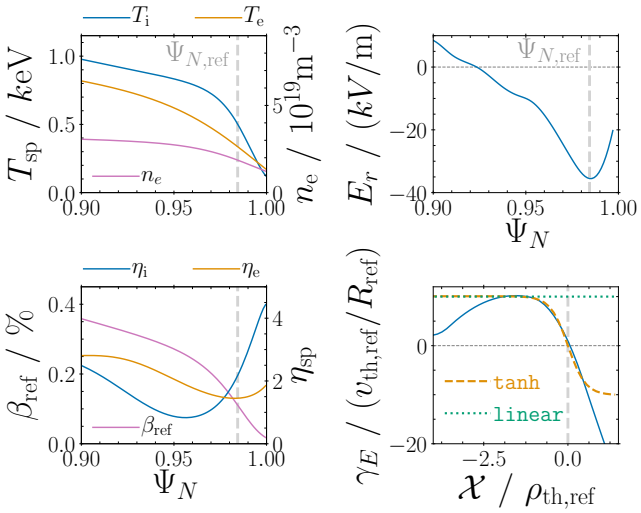

Fig. 1 Profiles from AUG shot #34548 (top and left panels) and $E \times B$ shear rate with fitted shear flow models (bottom right).

The impact of the edge E_r-well (Fig. 1) and the connected sheared $E \times B$ drift $\mathbf{u}_E = \mathbf{b} \times \nabla\Phi_0/B_0$, where $E_r = -\partial_r\Phi_0$, is modeled through two additional terms in the gyrokinetic equation $f_\mathrm{sp} \overset{+}{=} -\mathbf{u}_E \cdot \nabla f_\mathrm{sp}$ (advection by the background $E \times B$-drift) and $f_\mathrm{sp} \overset{+}{=} -(Z_\mathrm{sp} e v_\parallel/T_\mathrm{sp})(\mathbf{B}_1/B_0)\nabla\Phi_0 F_{\mathrm{M,sp}}$ (acceleration of gyrocenters in the electric field component parallel to radial magnetic field perturbations). Three different $E \times B$ shear flow models are fitted to the experimentally obtained $E \times B$ shear rate $\gamma_E = (1/B_\mathrm{ref})\partial_r^2\Phi_0$, from which Φ_0 entering the GK equation is obtained: (`tanh`) A tanh-shaped profile $\gamma_\mathrm{E} = \gamma_{\mathrm{E},0}\tanh[(r-r_{E,0})/\Delta r_E]$ with $\gamma_{\mathrm{E},0} = -10.0\ v_{\mathrm{th,ref}}/R_\mathrm{ref}$, $r_{E,0} = 0$ and $\Delta\mathcal{X}_{E,0} = \Delta r_{E,0}/\rho_{\mathrm{th,ref}} = 0.75$. (`linear`) A constant shear rate model $\gamma_\mathrm{E} = \gamma_{\mathrm{E},0} = -10.0$. (`tanh_ga`) Motivated by the narrow radial scale of the E_r-well on the order of the thermal Larmor radius and by more sophisticated edge gyrokinetic models [10] FLR effects are included into the tanh shear flow model by considering the gyroaveraged electrostatic potential $\mathcal{G}\{\Phi_0\}$ in the two additional terms entering the GK equation.

The MP in AUG #34548 satisfies $|\mathbf{B}_\mathrm{mp}|/|\mathbf{B}_0| \sim 10^{-4}$, which is consistent with the gyrokinetic ordering $|\mathbf{B}_1|/|\mathbf{B}_0| \sim \rho_*$ [11], and, therefore, the MP is modeled as a static part of the perturbed parallel vector potential $A_{1\parallel}$. Although the MP is usually composed of a poloidal spectrum [12], here only single helicity perturbations of the form $A_{1\parallel,\mathrm{mp}} = H(\nu)\cos[2\pi(n_\nu\nu - n_\gamma\gamma)]$ are considered, where γ and ν are toroidal and poloidal straight field line angles and n_γ and n_ν the corresponding mode numbers. $H(\nu)$ controls the (radially constant) amplitude, chosen to provide an experimentally relevant radial magnetic field perturbation $B_{1r,\mathrm{mp}}/B_\mathrm{ref} = 1.7 \times 10^{-4}$. The toroidal mode number of the MP is set to $n_\mathrm{mp} = 4$ and a finite parallel mode number $n_s = n_\nu - q_0 n_\gamma = 16$ is considered, such that the resonance position and the connected magnetic island is outside of the simulated domain. Crosschecks with $n_\mathrm{mp} = 2, 8$ and $n_s = 10, 12$ did not change the results presented here.

Axisymmetric study: Here, axisymmetry is assumed, limiting the validity to the transient phase just after the fast switch-off of the MP, where the plasma recovers axisymmetry but the profiles of density and temperature are still reasonably close to the ELM-suppressed state. The `linear` shear flow quenches the dominant slab ITG instability on ion scales (Fig. 2), while the tanh-shaped $E \times B$ shear flow models (`tanh` and `tanh_ga`) allow for finite slab ITG instability, highlighting the important role of a zero crossing in the $E \times B$ shear rate profile for instability. FLR effects (`tanh_ga`) mitigate the shear stabilization and even cause a slight destabilization in the range $n \approx 40 \sim 100$, with Eigenmodes localizing radially to the zero crossing of the $E \times B$ shear rate (Fig. 2). Slab ITG driven turbulence is sensitive to $\eta_\mathrm{i} = (R/L_{T\mathrm{i}})/(R/L_n)$ and a finite turbulent transport of ion heat Q_i and particles Γ_e occurs roughly for $\eta_\mathrm{i} \gtrsim 1$ (Fig. 3). Also in the nonlinear state the `linear` shear flow results in almost complete quenching, while the tanh-shaped models (`tanh` and `tanh_ga`) allow for finite turbulence, again pointing out the crucial role of the zero crossing. With FLR effects $E \times B$ shear stabilization is mitigated, which persists for a wider range of shear rate amplitudes (Fig. 3). Overall this demonstrates a lack of $E \times B$ shear stabilization of slab ITG turbulence provided the zero crossing of the $E \times B$ shear rate profile connected with the E_r-well and FLR effects are taken into account. An inversion of sign$(\gamma_{\mathrm{E},0})$ (labeled by `tanh_ga` (+)), i. e. a flipping of the radial symmetry of the tanh-shaped shear flow profile (bottom panels of Fig. 2) induces a strong reduction of the growth rate (see Fig. 2). Eigenmodes still localize to the zero crossing of the $E \times B$ shear rate profile, the detailed mode structures, however, depends on sign$(\gamma_{\mathrm{E},0})$, indicating a sign sensitive selection of the Eigenmodes. The inversion of sign$(\gamma_{\mathrm{E},0})$ causes also a significant reduction of the turbulence level (`tanh_ga` (+) in Fig. 3) compared to the experimentally relevant sign (`tanh_ga`).

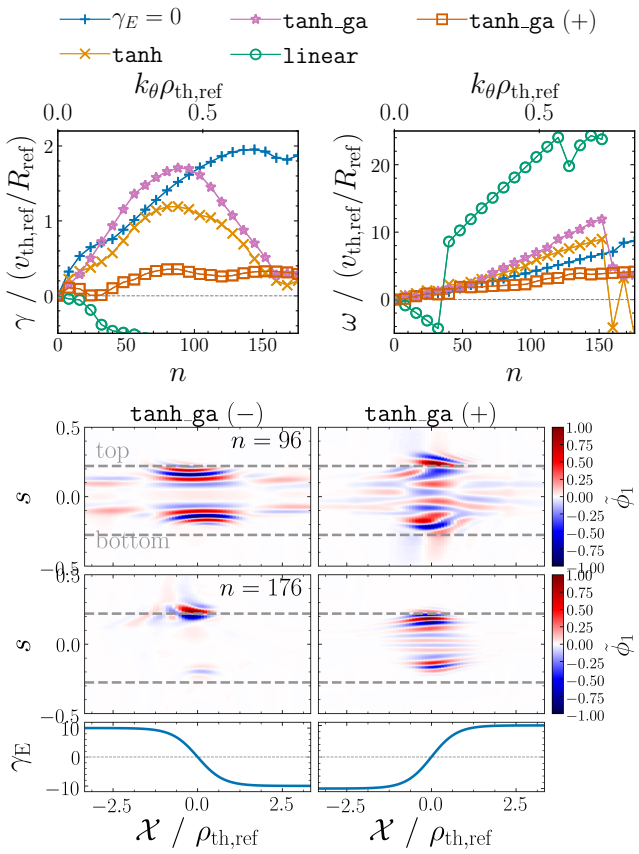

Fig. 2 Linear axisymmetric study: Growth rate γ and frequency ω spectra with different $E \times B$ shear flow models (top) and mode structure $\tilde{\phi}_1(\mathcal{X}, s)$ for different shear flow models and radial profiles of the $E \times B$ shear rate γ_E (bottom).

Non-axisymmetric study: Here, the simple single helicity MP with finite parallel mode number is imposed to make the plasma non-axisymmetric. First, the linear stability in the presence of a MP is studied by linearizing the gyrokinetic equation about the MP with the assumption that $A_{1\parallel}(n = n_\mathrm{mp}) = A_{1\parallel,\mathrm{mp}}$ and $f_{1\mathrm{sp}}(n = n_\mathrm{mp}) = \phi_1(n = n_\mathrm{mp}) = 0$. Due to the relaxation of axisymmetry all toroidal modes grow with a single growth rate $\gamma_{3\mathrm{d}}$ (left panel of Fig. 4) similar to Eigenmodes in stellarators [13, 14]. This MP coupled Eigenmode exhibits a typical mode number n_typ as indicated by the electrostatic potential power spectrum $P[\hat{\phi}_1]$. Variation of the maximum resolved toroidal mode number n_max allows to obtain a spectrum of MP coupled modes [14] (right panel of Fig. 4) and destabilization relative to the axisymmetric linear reference γ_ref is found. The typical toroidal mode number and the transport fingerprints (not shown) [15] are comparable to the dominant axisymmetric slab ITG,

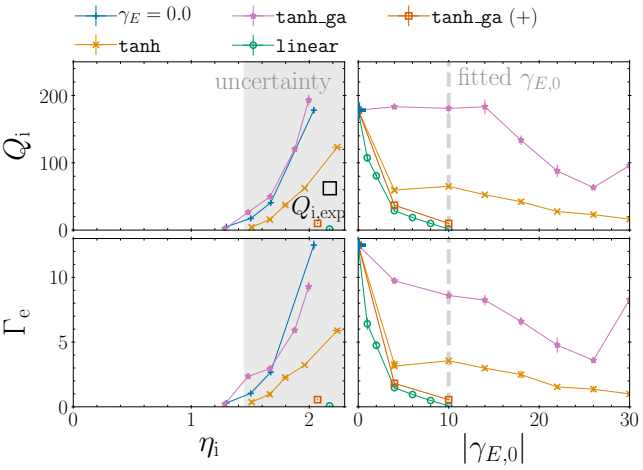

Fig. 3 Nonlinear axisymmetric study: Turbulent ion heat flux Q_i and electron particle flux Γ_e as function of η_i (left) and the $E \times B$ shear rate amplitude $\gamma_{\mathrm{E},0}$ (right) for different $E \times B$ shear flow models. The gray-shaded region depicts the experimental η_i values with their uncertainty.

indicating that the MP coupled Eigenmodes are of slab ITG type. The impact of MPs on turbulence is studied by restarting nonlinear axisymmetric simulations with the MP amplitude being ramped up linearly in time, reaching its target amplitude of $B_{1r,\mathrm{mp}}/B_{\mathrm{ref}} = 1.7 \times 10^{-4}$ at $\Delta t = 10\ v_{\mathrm{th,ref}}/R_{\mathrm{ref}}$ after restart (bottom left panel of Fig. 5). Here, the parallel vector potential in the $n = n_{\mathrm{mp}}$ toroidal mode is replaced by the magnetic perturbation $A_{1\parallel}(n = n_{\mathrm{mp}}) = A_{1\parallel,\mathrm{mp}}$, while the gyrocenter distribution function $f_{1\mathrm{sp}}(n = n_{\mathrm{mp}})$ and the electrostatic potential $\phi_1(n = n_{\mathrm{mp}})$ are allowed to evolve self-consistently in time. The turbulent ion heat flux Q_{i} and the electron particle flux Γ_{e} increase in response to the MP. The toroidal spectra of the turbulent fluxes (right panels of Fig. 5) exhibit increased Fourier amplitudes for same toroidal Fourier modes $n \gtrsim 50$ corresponding to the destabilized MP coupled Eigenmodes (Fig. 4). This suggests that the destabilization of ion scale MP coupled Eigenmodes of slab ITG character is partly the reason for the augmented turbulence level.

Discussion: The lack of $E \times B$ shear stabilization of slab ITG turbulence appears to be in contradiction with the general understanding that ITG driven turbulence is likely stabilized by the $E \times B$ shear connected with the E_r-well [16,17]. First, as mentioned in a recent global gyrokinetic study of pedestal slab ITG turbulence [18], a zero crossing in the $E \times B$ shear rate results in the nontrivial dependence of turbulence on the shear rate amplitude, i. e., a deviation of the turbulence transport scaling from conventional shear stabilization models [19], which assume an $E \times B$ shear flow with constant $E \times B$ shear rate. The present study confirms the crucial role of a zero crossing for linear stability (Fig. 2) and turbulence (Fig. 3). Second, and in contrast to previous works, here FLR corrections to the background $E \times B$ drift are incorporated, which is consistent with more sophisticated edge specific gyrokinetic frameworks [10]. Especially ions then experience an effective background $E \times B$ drift with reduced $E \times B$ shear rate, which is in line with a mitigation of shear stabilization. Note, however, that at sufficiently large $E \times B$ shear rates, the tanh-shaped $E \times B$ shear flow with both zero crossing and gyroaverage still acts stabilizing (Fig. 3), suggesting that the concept of shear stabilization still applies. The lack of shear stabilization of slab ITG turbulence implies that slab ITG turbulence might be a proper candidate for controlling the profiles of ion temperature and density in H-mode edges, provided the conditions $\eta_{\mathrm{i}} \gtrsim 1$ (ITG instability condition) and $R/L_{T\mathrm{i}} \gg 1$ (slab resonance) are met. The sensitivity of both linear stability and turbulence on the radial symmetry of the $E \times B$ shear rate profile and, hence, the $E \times B$ flow curvature, appears to be in agreement with previous works pointing out the role of the E_r curvature for slab ITG instability [20]. However, the aforementioned reference finds that a positive curvature (E_r-well) acts stabilizing on slab ITG, which is contrary to the present study (see Fig. 2). This discrepancy is likely related to the difference of the simple 1D kinetic model considered in Ref. [20] and the present more sophisticated gyrokinetic model. A comparison of the experimental heating power evaluated at the experimental η_{i} (black square in Fig. 3) with the modeled turbulent transport and assuming an uncertainty of ±20 % in both $R/L_{T\mathrm{i}}$ and R/L_n (gray-shaded region in Fig. 3) suggests that just after the fast switch-off of the MP the steep ion temperature gradient zone of AUG #34548 is likely close to the slab ITG turbulence threshold. This is further supported by the lack of $E \times B$ shear stabilization and the stiffness of the transport with respect to η_{i}. The properties of the slab ITG instability and turbulence, i. e., unstable in the steep gradient zone, propagation in the ion diamagnetic direction, structures on ion Larmor radius scales $k_\theta \rho_{\mathrm{th,ref}} \sim 10^{-1}$ and finite particle transport, as well as the destabilization by MPs are consistent with properties of the broadband density fluctuations observed in Ref. [2]. Slab ITG turbulence is, hence, a potential candidate for the broadband density fluctuations and the related turbulent particle transport might partly cause the density-pump out. This notion is further supported by another experimental observation: The density pump-out is usually a two step process, composed of a first density pump-out, which reduces the pedestal top density while the ion and electron pedestal top temperature remain mostly unchanged, and a subsequent second pump-out, accompanied by a reduction of the ion and electron temperature, further reducing the density below the ELM suppression threshold [2]. One may speculate that the first pump-out brings the edge profiles to the slab ITG turbulence threshold by increasing η_i through a reduction of R/L_n. Then, MP destabilized slab ITG turbulence might cause heat and particle transport manifesting itself in the second density pump-out.

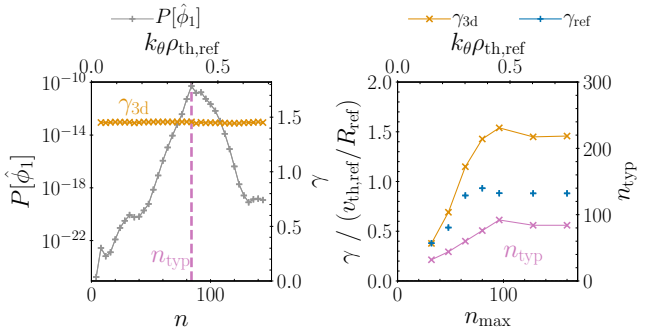

Fig. 4 Linearized non-axisymmetric study: Growth rate $\gamma_{3\mathrm{d}}$ and toroidal power spectrum of MP coupled mode (left) as well as growth rate $\gamma_{3\mathrm{d}}$ and typcial mode number n_{typ} as function of the maximum resolved toroidal mode number n_{max}. The growth rate from an axisymmetric linear reference simulation is depicted by γ_{ref}.

Conclusion: Within a local gyrokinetic study of the edge of the ELM suppressed H-mode AUG shot #34548 several results have been obtained: (i) $E\times B$ shear stabilization of slab ITG instability and turbulence is mitigated when FLR effects and a zero crossing of the $E \times B$ shear rate are taken into account in the background $E \times B$ shear flow model connected with the E_r-well. Both a zero crossing and FLR corrections are, hence, crucial for the description of slab ITG turbulence in steep gradient zones of H-modes. (ii) In the presence of an inhomogeneous $E \times B$ shear flow compliant with the shape of the E_r-well, slab ITG instability and turbulence is highly sensitive to the sign of the $E\times B$ shear rate, i. e., the radial symmetry of the $E \times B$ shear flow profile. (iii) Single helicity magnetic perturbations with finite parallel mode number destabilize slab ITG instability and turbulence.

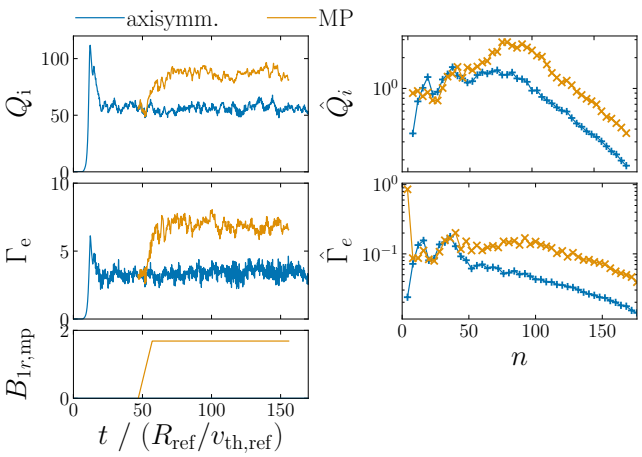

Fig. 5 Nonlinear non-axisymmetric study: Time traces of the turbulent ion heat flux Q_i, electron particle flux Γ_e and MP field amplitude $B_{1r,\mathrm{mp}}$ (left) and toroidal flux spectra (right) of an axisymmetric reference simulation (blue) and a non-axisymmetric case with addition of a MP.

The above findings point towards a potential role of slab ITG turbulence for the observed broadband density fluctuations in ELM-suppressed H-modes [2]. Clearly the local approximation considered in this study is inconsistent with the steep gradient zone and an investigation of the findings above within a radially global gyrokinetic approach is highly desired and currently pursued. Initial results qualitatively confirm the first two of the results summarized above, while global simulations with MPs remain numerically challenging. Ultimately, a full-f gyrokinetic model including the X-point and the scrape off layer such as XGC [21] or GENE-X [22] is required to properly test the findings above.

References

[1] W. Suttrop *et al*, Nucl. Fusion **58**, 096031 (2018).
[2] N. Leuthold, *et al*, Nuclear Fusion **63**, 046014 (2023).
[3] G. McKee, *et al*, Nucl. Fusion **53**, 113011 (2013).
[4] Jaehyun Lee, *et al*, Phys. Rev. Lett. **117**, 075001 (2016).
[5] R. Hager, C. S. Chang, N. M. Ferraro and R. Nazikian, Phys. Plasmas **27**, 062301 (2020).
[6] A. G. Peeters, *et al*, Comput. Phys. Commun **180**, 2650-2672 (2009).
[7] D.R. Hatch, M. Kotschenreuther, S. Mahajan, P. Valanju and X. Liu, Nucl. Fusion **57** 036020 (2017).
[8] R. Arbon, J. Candy and E. A. Belli, Plasma Phys. Control. Fusion **63**, 012001 (2020).
[9] R. E. Waltz and R. L. Miller, Phys. Plasmas **6**, 4265–4271 (1999).
[10] G. Kawamura and A. Fukuyama, Phys. Plasmas **15**, 042304 (2008).
[11] A. J. Brizard and T. S. Hahm, Rev. Mod. Phys. **79**, 421 (2007).
[12] D. A. Ryan *et al* Plasma Phys. Control. Fusion **57**, 095008 (2015).
[13] E. Sánchez, *et al*, Nucl. Fusion **61** 116074 (2021).
[14] F. Wilms, *et al*, J. Plasma Phys. **87**, 905870604 (2021).
[15] M. Kotschenreuther, *et al*, Nuclear Fusion **59**, 096001 (2019).
[16] H. Biglari, P. H. Diamond, and P. W. Terry, Physics of Fluids B **2**, 1 (1990).
[17] K. H. Burrell, Phys. Plasmas **4**, 14991518 (1997).
[18] D. R. Hatch, R. D. Hazeltine, M. K. Kotschenreuther and S. M. Mahajan, Plasma Phys. Control. Fusion **60**, 084003 (2018).
[19] Y. Z. Zhang, S. M. Mahajan, Phys. Fluids B **4**, 1385–1387 (1992).
[20] G.M. Staebler and R.R. Dominguez, Nucl. Fusion **31**, 1891 (1991).
[21] S. Ku, *et al*, J. Phys. Conf. Ser. **46**, 87 (2006).
[22] D. Michels, A. Stegmeir, P. Ulbl, D. Jarema, and F. Jenko, Comput. Phys. Commun. **264**, 107986 (2021).